STRUCTURE AND NOISE CHARACTERISTICS OF TURBULENT FLOW OVER A SPHERE

Giwoong Yun
School of Mechanical and Aerospace Engineering,
Seoul National University
Seoul 151-744, Korea

Dongjoo Kim
Center for Turbulence and Flow Control Research,
Institute of Advanced Machinery and Design
Seoul National University
Seoul 151-744, Korea

Haecheon Choi
School of Mechanical and Aerospace Engineering,
Seoul National University
Seoul 151-744, Korea
choi@socrates.snu.ac.kr

ABSTRACT

Numerical simulations of flow around a sphere are conducted at two different Reynolds numbers (Re = 3700 and 10^4) based on the freestream velocity and the sphere diameter. The numerical method used for obtaining the flow over a sphere is based on an immersed boundary method in a cylindrical coordinate system. At Re = 3700, the shear layer is elongated in the streamwise direction to form a cylindrical vortex sheet and its instability appears at $x/d \approx 2$. The flow behind the sphere is nearly laminar at $x/d < 1$ and contains few vortices there. On the other hand, for $Re = 10^4$ the shear-layer instability occurs right behind the sphere in the form of vortex tube and the flow becomes turbulent in the near wake. Therefore, at $Re = 10^4$, the size of the recirculation region is smaller and the wake recovers more quickly than that at Re = 3700. It is shown using the particle tracing and vortex identification method that the shear-layer and wake instabilities are closely related to each other. In order to investigate the acoustic field around the sphere, the Curle's solution of the Lighthill acoustic analogy is applied. With the far-field and compact-source approximation, the acoustic source in flow around a sphere is regarded as a point source. Due to the three-dimensional vortical evolution in the wake, the acoustic field evolves in a complicated manner, which is very different from that from flow over a cylinder.

INTRODUCTION

Flow structure and flow-induced noise around a sphere in a uniform flow are of central interest in many engineering applications because the sphere is a representative bluff body. However, their characteristics have not been well understood as compared to those around a circular cylinder. Previous studies on flow over a sphere have been mostly based on experimental methods, where vortical structures behind the sphere were identified using flow visualization and the high and low frequency characteristics in the shear layer were obtained using a single hot-wire measurement (Kim and Durbin 1988; Sakamoto and Haniu 1990). Recently, only a few numerical studies have been made on turbulent flow over a sphere (Tomboulides 1993; Constantinescu and Squires 2000). However, the qualitative and quantitative information on the turbulence statistics behind the sphere is still limited in the literature, and thus the flow-induced noise from flow over a sphere has not been studied in detail. Therefore, the objectives of the present study are to investigate the characteristics of turbulent flow over a sphere such as a separating shear layer, turbulence statistics and wake structures, and to predict the flow-induced noise using the flow-field information and Lighthill's acoustic analogy.

The present numerical method for solving the incompressible Navier-Stokes equations is based on an immersed boundary method in a cylindrical coordinate, where the momentum forcing and mass source are provided at grid points inside the sphere to satisfy the no-slip boundary condition on the sphere surface (Kim et al. 2001). Large eddy simulation with a dynamic subgrid-scale model (Germano et al. 1991; Lilly 1992) is conducted at two different Reynolds numbers of $Re = u_\infty d/\nu = 3700$ and 10^4, where u_∞ is the freestream velocity and d is the sphere diameter. The computational domain used is $-15 \le x/d \le 15$, $0 \le r/d \le 15$, $0 \le \phi < 2\pi$, and the number of grid points is 577 (x) $\times$ 141 (r) $\times$ 40 (ϕ). Here, x, r and ϕ denote, respectively, the streamwise, radial and azimuthal directions. A Cartesian coordinate system (x, y, z) is also used in order to define the drag and lift forces, where the lift force is composed of two orthogonal (y and z) components. In order to investigate the acoustic field around the sphere, the Curle's solution (1955) of the Lighthill acoustic analogy (1952) is applied.

ACOUSTIC ANALOGY

Lighthill (1952) formulated a linear, inhomogeneous wave equation from the exact equations of fluid motion and showed that an unsteady flow region in an unbounded domain is acoustically equivalent to a distribution

Table 1: Flow parameters of turbulent flow over a sphere: Exp^1, Kim and Durbin (1988); Exp^2, Sakamoto and Haniu (1990); $Comp^1$, Constantinescu and Squires (2000).

	Re	$\bar{C}_d$	$\bar{C}_{p_b}$	St	$\bar{\alpha}_s$
Present	3700	0.36	-0.20	0.22	90^o
(LES)	10^4	0.40	-0.28	0.18	90^o
Exp^1	3700			0.22	
	4200		-0.23		
	10^4			0.16	
Exp^2	3700			0.21	
	10^4			0.18	
$Comp^1$					
(LES)	10^4	0.393		0.195	$84^o - 86^o$
(DES)	10^4	0.397		0.200	$84^o - 87^o$

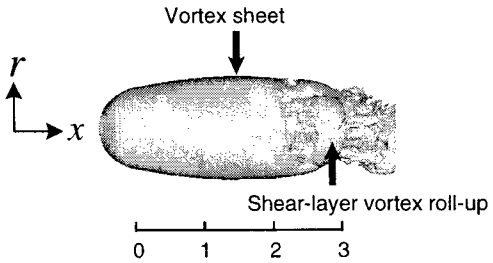

(a)

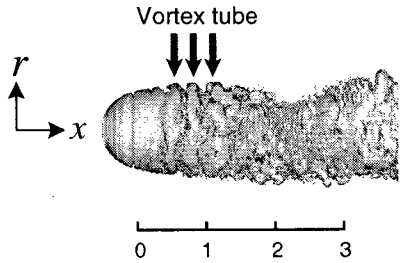

(b)

Figure 1: Vortical structure in the near wake: (a) $Re = 3700$; (b) $Re = 10^4$.

of quadrupole sources. When a solid body is present in the flow, Curle's integral solution (1955) to the Lighthill equation provides a theoretical framework for predicting the noise of flow-body interaction. Also, in the case that the distance between observation and source points is larger than the acoustic wavelength, the far-field approximation can be applied. Furthermore, when the solid body and the source region are smaller than the typical wavelength, the source region can be regarded as a compact-source region. Thus, the acoustic density $(\rho_c - 1)$ or noise at the far field produced from a compact-source region is approximated by

$$\rho_c(\bar{x},t) - 1 = \frac{M^3}{4\pi}\frac{x_i}{x^2}\frac{\partial}{\partial t}\int_S n_j P_{ij}(\bar{y}, t - Mx)d^2\bar{y} + \frac{M^4}{4\pi}\frac{x_i x_j}{x^3}\frac{\partial^2}{\partial t^2}\int_V T_{ij}(\bar{y}, t - Mx)d^3\bar{y}, \quad (1)$$

where

$$T_{ij} = \rho u_i' u_j' + p\delta_{ij} - \frac{1}{M^2}\rho\delta_{ij} - \tau_{ij}, \quad (2)$$

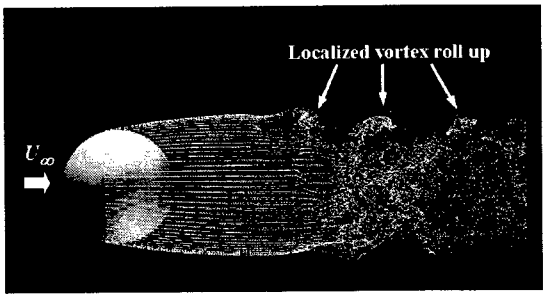

(a)

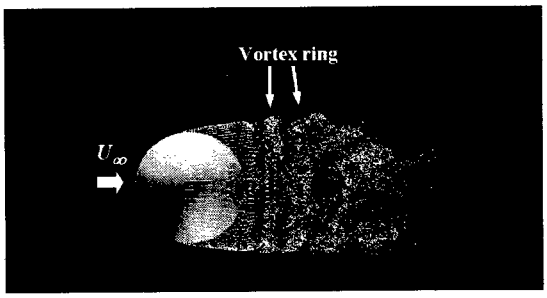

(b)

Figure 2: Flow structures in the near wake using particle tracing: (a) $Re = 3700$; (b) $Re = 10^4$.

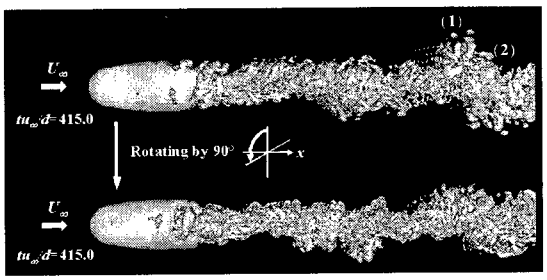

(a)

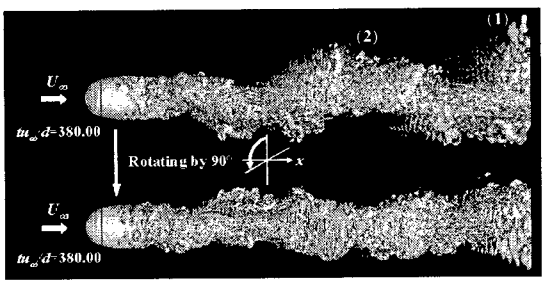

(b)

Figure 3: Instantaneous vortical structures on two perpendicular planes: (a) $Re = 3700$; (b) $Re = 10^4$.

$$\tau_{ij} = \frac{1}{Re}\left(\frac{\partial u_i'}{\partial x_j} + \frac{\partial u_j'}{\partial x_i} - \frac{2}{3}\delta_{ij}\frac{\partial u_k'}{\partial x_k}\right), \quad (3)$$

$$P_{ij} = p\delta_{ij} - \tau_{ij} \quad (4)$$

and

$$u_i' = u_i - U_\infty\delta_{1i}. \quad (5)$$

Here M is the freestream Mach number, T_{ij} is the Lighthill stress tensor, τ_{ij} is the viscous stress tensor, the prime $(\cdot)'$

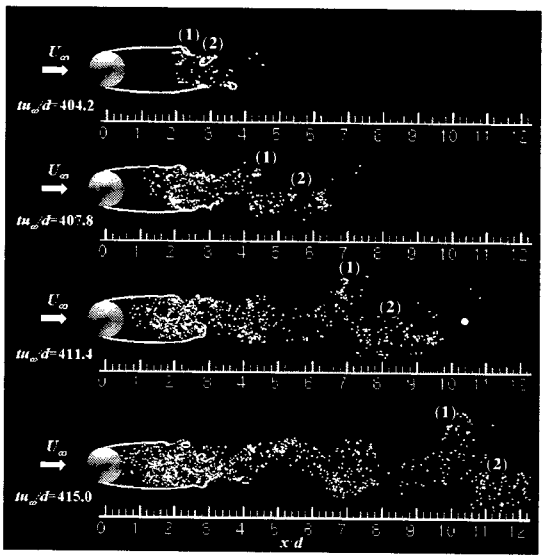

(a)

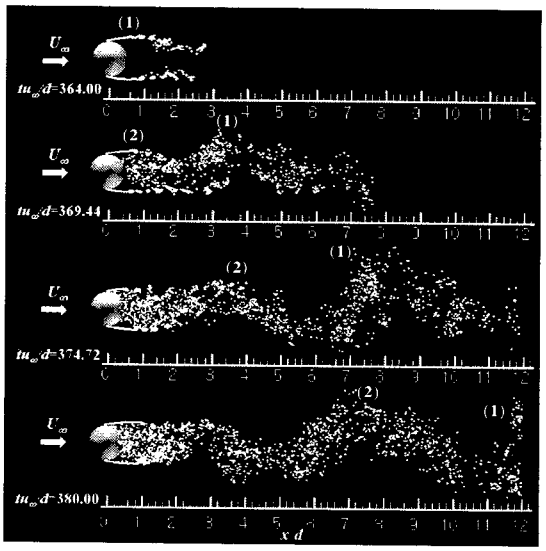

(b)

Figure 4: Time sequence of vortical structures with particle tracing: (a) $Re = 3700$; (b) $Re = 10^4$.

denotes the fluctuation quantity, $\bar{x}$ is the observation point vector, $\bar{y}$ is the source point vector, $x = \mid \bar{x} \mid$, n_j is the directional cosine of the vector outward normal to a solid surface, V is the computational domain and S is the sphere surface.

Equation (1) includes two typical acoustic source functions: a surface dipole and a volume quadrupole that are generated from the surface of a sphere and the entire unsteady flow region, respectively. The Mach number dependence of the volume quadrupole is $O(M)$ times larger than that of the surface dipole. In this study, $\dot{D}_i$ and $\ddot{Q}_{ij}$ denote the dipole and quadrupole source functions, respectively:

$$\dot{D}_i(t) = \frac{\partial}{\partial t} \int_S n_j P_{ij}(\bar{y}, t - Mx) d^2\bar{y}, \tag{6}$$

$$\ddot{Q}_{ij}(t) = \frac{\partial^2}{\partial t^2} \int_V T_{ij}(\bar{y}, t - Mx) d^3\bar{y}. \tag{7}$$

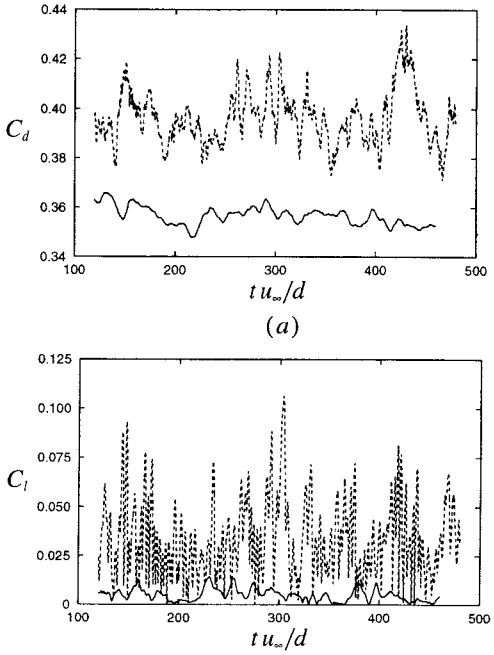

Figure 5: Drag and lift coefficients: (a) drag; (b) lift. ——, $Re = 3700$; – – – –, $Re = 10^4$.

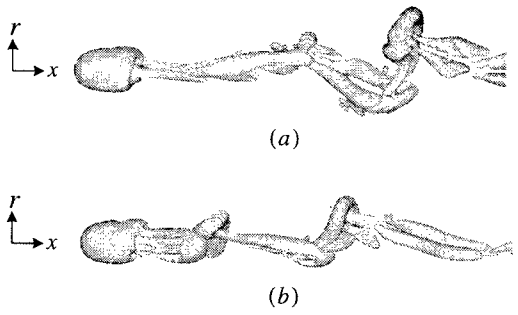

Figure 6: Instantaneous vortical structures at $Re = 425$: (a) $tu_\infty/d = 543.2$; (b) $tu_\infty/d = 555.0$.

RESULT

Flow field

The present simulation results are summarized in table 1, together with those from the previous experimental and numerical studies. In table 1, $\bar{C}_d$ denotes the time-averaged drag coefficient, $\bar{C}_{pb}$ the base-pressure coefficient, $\bar{\alpha}_s$ the separation angle, and St the Strouhal number associated with the wake instability. Also, in table 1 LES and DES denote large eddy simulation and detached eddy simulation, respectively, and DES is a hybrid approach reducing to Reynolds-averaged Navier-Stokes simulation (RANS) near the wall and LES away from the wall. It is shown in table 1 that the present results are in good agreement with the previous ones. Note that $\bar{C}_d$ at $Re = 3700$ is smaller than that at $Re = 10^4$, which is consistent with the variation of the base-pressure coefficient with the Reynolds number.

Figure 1 shows instantaneous vortical structures in the near wake, where the vortical surfaces are identified using

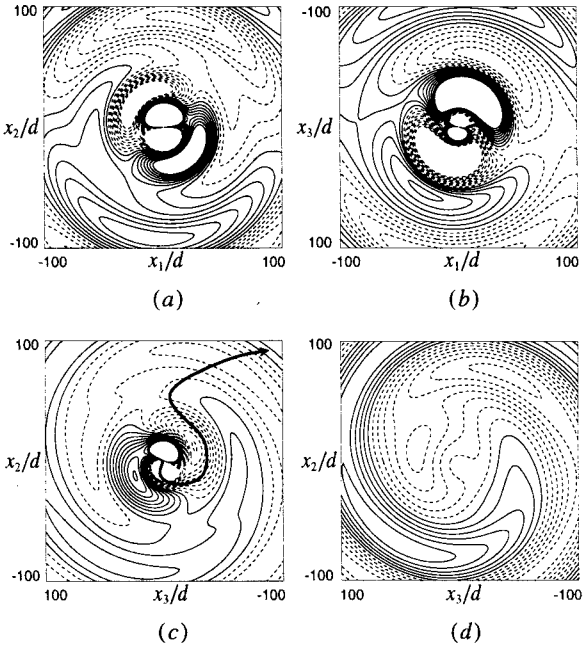

Figure 7: Contours of the noise due to dipole source at $Re = 425$ and $M = 0.1$: (a) $x_1 - x_2$ plane ($x_3 = 0$); (b) $x_1 - x_3$ plane ($x_2 = 0$); (a) $x_3 - x_2$ plane ($x_1 = 0$); (a) $x_3 - x_2$ plane ($x_1 = 50$). Maximum values are fixed as 4.58×10^{-8} in (a), (b) and (c), and 1.58×10^{-8} in (d).

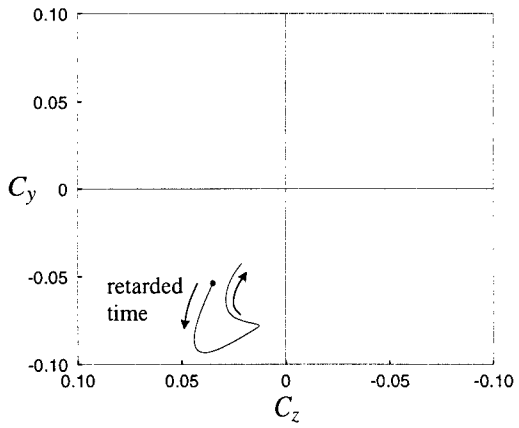

Figure 8: Phase diagram (C_y, C_z) at $Re = 425$.

the method by Jeong and Hussain (1995). At $Re = 3700$, the shear layer is elongated in the streamwise direction to form a cylindrical vortex sheet and its instability becomes manifest at $x/d \approx 2$. The flow right behind the sphere is nearly laminar. On the other hand, at $Re = 10^4$, the shear-layer instability occurs right behind the sphere in the form of vortex tube and the flow becomes turbulent in the near wake. Therefore, at $Re = 10^4$, the size of the recirculation region is smaller and the wake recovers more quickly than at $Re = 3700$.

Figure 2 shows the vortex roll up in the shear layer at $Re = 3700$ and $Re = 10^4$ using particle tracing. For $Re = 3700$, the vortices roll up locally in the azimuthal direction near the end of the shear layer, whereas for $Re = 10^4$ vortex rings are formed right behind the sphere.

Figure 3 shows the instantaneous vortical structures at

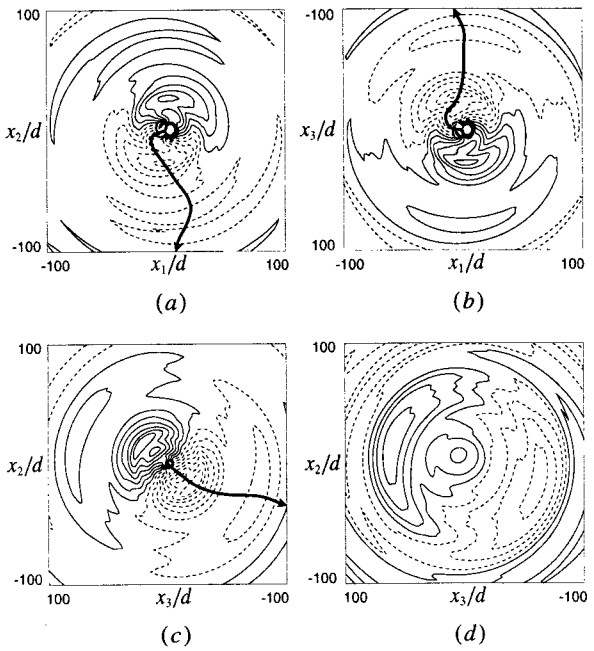

Figure 9: Contours of the noise due to dipole source at $Re = 3700$ and $M = 0.1$: (a) $x_1 - x_2$ plane ($x_3 = 0$); (b) $x_1 - x_3$ plane ($x_2 = 0$); (a) $x_3 - x_2$ plane ($x_1 = 0$); (a) $x_3 - x_2$ plane ($x_1 = 50$). Maximum values are fixed as 7.51×10^{-9} in (a), (b) and (c), and 2.51×10^{-9} in (d).

$tu_\infty/d = 415.0$ ($Re = 3700$) and $tu_\infty/d = 380.00$ ($Re = 10^4$) using the vortex identification method by Jeong and Hussain (1995). One can clearly notice that alternating vortical structures exist in one plane but do not appear in the perpendicular plane. In order to understand this phenomenon, time traces of vortical structures are shown using particle tracing in figure 4, where particles are released at two (upper and lower) points very near the sphere surface. The vortices, (1) and (2), that are generated by the shear-layer instability persist in the far-downstream locations, resulting in the waviness of the wake structure. Therefore, it can be concluded that the wake instability is closely associated with the shear-layer instability for flow over a sphere.

Acoustic field

At low Mach number the dominant acoustic sources are the temporal variations of drag and lift on the surface of a sphere, as expected from equation (1). Figure 5 shows the variations of drag ($C_d = C_x$) and lift coefficients ($C_l = \sqrt{C_y^2 + C_z^2}$) at $Re = 3700$ and 10^4. The variations of C_d and C_l at $Re = 10^4$ are larger than those at $Re = 3700$. Since the lift fluctuations are also larger than the drag fluctuations at both Reynolds numbers, it is expected that the intensity of far-field noise from the lift fluctuations are larger than that from the drag fluctuations.

In order to understand the characteristics of the flow-induced noise, we first consider a relatively low Reynolds number of $Re = 425$ and $M = 0.1$. At this Reynolds number, the vortical structures are completely unsteady and three-dimensional, but the shear-layer instability observed at $Re = 3700$ and 10^4 is absent (figure 6). Figure 7 shows the contours of the dipole noise due to the drag and lift fluctuations. Since the drag and lift change irregularly in time even for $Re = 425$, the noise propagates into all directions in

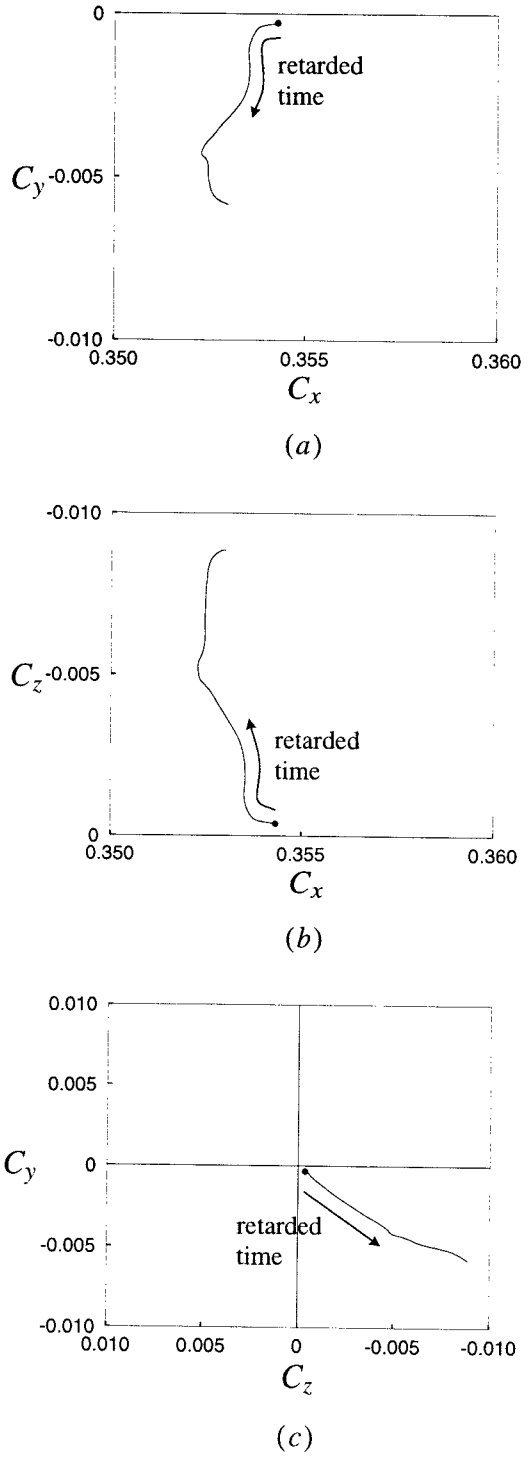

Figure 10: Phase diagrams at $Re = 3700$: (a) C_x vs. C_y (b) C_x vs. C_z; (c) C_y vs. C_z.

a complicated manner. The noise due to C_y and C_z on an $x_2 - x_3$ plane is shown in figure 7(c), where the direction of noise propagation follows the direction of time on the phase diagram of C_y and C_z (see figure 8).

Figure 9 shows the contours of the noise due to the drag and lift fluctuations for $Re = 3700$ and $M = 0.1$. Figure 9(a) shows the noise propagation from C_x and C_y, figure 9(b) from C_x and C_z, and figure 9(c) from C_y and C_z, respectively. Therefore, as seen from this figure, the noise due

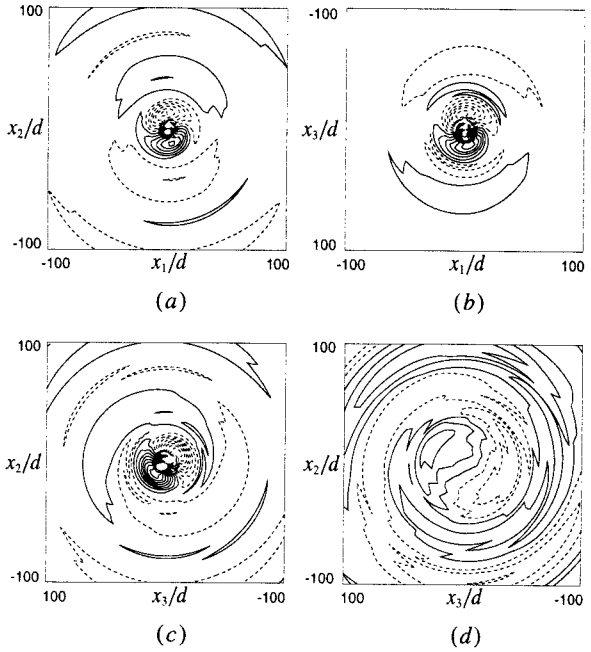

Figure 11: Contours of the noise due to dipole source at $Re = 10^4$ and $M = 0.1$: (a) $x_1 - x_2$ plane ($x_3 = 0$); (b) $x_1 - x_3$ plane ($x_2 = 0$); (a) $x_3 - x_2$ plane ($x_1 = 0$); (a) $x_3 - x_2$ plane ($x_1 = 50$). Maximum values are fixed as 2.81×10^{-7} in (a), (b) and (c), and 7.81×10^{-8} in (d).

to lift fluctuations is much larger than that due to drag fluctuations. The direction of noise propagation also follows the direction of time on the phase diagrams (see figure 10). The noise from C_y and C_z is shown at $x_1/d = 50$ in figure 9(d), where the directivity of the noise from the lift fluctuations is almost maintained as compared to that at $x_1 = 0$ (see figure 9c). Also, the circular-shaped contours in this figure indicate that the noise from the drag fluctuations little influences the total noise.

Figure 11 shows the contours of the noise due to the drag and lift fluctuations for $Re = 10^4$. The noise propagation at $Re = 10^4$ is more complicated than that at $Re = 3700$ and the acoustic intensity is much larger at $Re = 10^4$ than that at $Re = 3700$.

CONCLUSION

Numerical simulations of flow around a sphere were conducted at $Re = 3700$ and 10^4. The present simulation results such as the drag coefficient, base-pressure coefficient, separation angle and Strouhal number were in good agreement with the previous experimental and numerical ones. It was found that the wake instability was closely associated with the shear-layer instability for flow over a sphere and the vortices that were generated by the shear-layer instability resulted in the waviness of the wake structure.

The far-field and compact-source approximation for the Curle's solution of the Lighthill acoustic equation was adopted to predict the noise from flow behind a sphere. Since the drag and lift changed irregularly in time for both Reynolds numbers, the noise propagated in a complicated manner. The noise due to the lift fluctuations was much larger than that due to the drag fluctuations. The direction of noise propagation followed the direction of time on the phase diagram between the drag and lift forces.

ACKNOWLEDGEMENTS

This work is supported by the Creative Research Initiatives of the Korean Ministry of Science and Technology.

REFERENCES

Constantinescu, G. S. and Squires, K. D., 2000, "LES and DES Investigations of Turbulent Flow over a Sphere", *AIAA paper*, 2000-0540.

Curle, N., 1955, "The Influence of Solid Boundaries upon Aerodynamic Sound", *Proceedings of the Royal Society of London, Series A: Mathematical and Physical Sciences*, Vol. 231, pp. 505-514.

Germano, M., Piomelli, U., Moin, P. and Cabot, W. H., 1991, "A Dynamic Subgrid-Scale Eddy Viscosity Model", *Physics of Fluids*, Vol. 3, pp. 1760-1765.

Jeong, J. and Hussain, F., 1995, "On the Identification of a Vortex", *Journal of Fluid Mechanics*, Vol. 285, pp. 69-94.

Kim, H. J. and Durbin, P. A., 1988, "Observations of the Frequencies in a Sphere Wake and of Drag Increase by Acoustic Excitation", *Physics of Fluids*, Vol. 31, pp. 3260-3265.

Kim, J., Kim, D. and Choi, H., 2001, "An Immersed-Boundary Finite Volume Method for Simulations of Flow in Complex Geometries", *Journal of Computational Physics*, Vol. 171, pp. 132-150.

Lighthill, M. J., 1952, "On Sound Generated Aerodynamically: I. General Theory", *Proceedings of the Royal Society of London, Series A: Mathematical and Physical Sciences*, Vol. 211, pp. 564-587.

Lilly, D. K., 1992, "A Proposed Modification of the Germano Subgrid-Scale Closure Method", *Physics of Fluids*, Vol. 4, pp. 633-635.

Sakamoto, H. and Haniu, H., 1990, "A Study on Vortex Shedding from Spheres in a Uniform Flow", *Journal of Fluid Engineering*, Vol. 112, pp. 386-392.

Tomboulides, A., 1993, "Direct and Large-Eddy Simulation of Wake Flows: Flow past a Sphere", PH.D. dissertation, Princeton University.